Low-Complexity Massive MIMO Tensor Precoding

Lucas N. Ribeiro[*], *Stefan Schwarz*[†], *André L. F. de Almeida*[‡], *Martin Haardt*[*]
[*]Communications Research Laboratory, Technische Universität (TU) Ilmenau, Ilmenau, Germany
[†]Christian Doppler Laboratory for Dependable Wireless Connectivity for the Society in Motion, TU Wien, Vienna, Austria
[‡]Wireless Telecommunications Research Laboratory, Federal University of Ceará, Fortaleza, Brazil

***Abstract*—We present a novel and low-complexity massive multiple-input multiple-output (MIMO) precoding strategy based on novel findings concerning the subspace separability of Rician fading channels. Considering a uniform rectangular array at the base station, we show that the subspaces spanned by the channel vectors can be factorized as a tensor product between two lower dimensional subspaces. Based on this result, we formulate tensor maximum ratio transmit and zero-forcing precoders. We show that the proposed tensor precoders exhibit lower computational complexity and require less instantaneous channel state information than their linear counterparts. Finally, we present computer simulations that demonstrate the applicability of the proposed tensor precoders in practical communication scenarios.**

***Index Terms*—Massive MIMO, tensors, precoding**

I. Introduction

Massive multiple-input multiple-output (MIMO) is one of the main enabling technologies for 5G networks. It consists of employing many active antennas at the base station (BS) to serve multiple users on the same time-frequency resource [1]. It can provide high data throughput by spatial signal processing at the BS (precoding) to combat multi-user interference and to provide large beamforming gains. Maximum ratio transmission (MRT) and zero-forcing (ZF) precoding are known to perform well if accurate instantaneous channel state information (CSI) is available at the BS. However, in practice, CSI estimates are often noisy, since accurate estimation of the high-dimensional massive MIMO channels can be quite expensive in terms of power and time-frequency resources. Moreover, the ZF precoder is known to be computationally expensive due to the large number of computations it requires to invert the high-dimensional channel Gram matrix [2].

Several solutions have been proposed to simplify the CSI requirements and to reduce the computational complexity of massive MIMO precoders. An efficient solution consists of designing precoders based on partial CSI [3]–[5]. This kind of CSI is typically less expensive to estimate than full instantaneous CSI. To reduce the computational complexity of the precoder design, many strategies are available in the literature. For example, series expansion techniques [6], precoder interpolation [7], decentralized filtering [8], and multi-layer filtering [9], [10]. Different approaches that exploit the algebraic properties of the MIMO channel to reduce both CSI requirements and computational complexity have been investigated in the literature [11]–[16]. In some conditions, the channel may be well-approximated by the tensor product between lower dimensional components. This allows us to develop low-complexity tensor filters.

Tensor filtering has been applied to system identification [11] and equalization problems [12]–[14]. A common aspect among these works is the separable system model, i.e., the vector or matrix that models the system can be exactly factorized in terms of tensor products. In [11]–[14], we have developed low-complexity tensor filtering schemes that exploit this property to reduce the number of calculations involved in the filter design. However, strict separability is rarely encountered in practice due to the non-separable nature of many devices and physical phenomena, limiting the applicability of the previously proposed filtering methods.

In this paper, we adopt a different approach to our previous works. Instead of assuming simplified separable models, we consider a practical channel model and demonstrate that, under some conditions, the subspaces spanned by the channel vectors can be factorized into a tensor product between lower dimensional subspaces. More specifically, we consider a BS equipped with a uniform rectangular array (URA) and we assume Rician fading channels. We show that the subspace spanned by the channel vectors can be decomposed into the tensor product between the subspaces spanned by the BS horizontal and vertical linear sub-arrays. Based on this result, we formulate the tensor maximum ratio transmission (TMRT) and tensor zero-forcing (TZF) precoders. These tensor precoders are based on low-dimensional instantaneous CSI. Therefore, they are less expensive to estimate than the full high-dimensional CSI required by the classical MRT and ZF precoders. Moreover, they require much less computational resources than their classical counterparts. For example, we show that the runtime of TZF is twice as fast as that of ZF while the achievable sum-rate difference is minimal.

The proposed precoders are related to the techniques discussed in [15], [16]. The work of [15] proposes a precoder scheme that exploits the geometry of URAs by means of the Kronecker (tensor) product to reduce the design complexity. Likewise, [16] leverages the tensor product in the design of analog beamformers to null undesired signals. We emphasize that the present paper extends the contributions of [15], [16] by providing novel theoretical results about the channel subspace separability. Moreover, we show when these results can be applied to reduce the CSI requirements and the computational complexity of the proposed precoding methods considering a practical dynamical scenario.

Notation: Vectors and matrices are written as lowercase and uppercase boldface letters, respectively. The transpose and the conjugate transpose (Hermitian) of $\boldsymbol{X}$ are represented by $\boldsymbol{X}^{\mathsf{T}}$ and $\boldsymbol{X}^{\mathsf{H}}$, respectively. The N-dimensional identity matrix is represented by $\boldsymbol{I}_N$ and the $(M \times N)$-dimensional null matrix by $\mathbf{0}_{M\times N}$. The symbol $\delta(\cdot)$ denotes the Kronecker's delta function. The $\mathrm{Diag}(\cdot)$ operator transforms an input vector into a diagonal matrix, $\mathrm{span}(\cdot)$ refers to the subspace spanned by the argument vectors, $O(\cdot)$ stands for the Big-O complexity

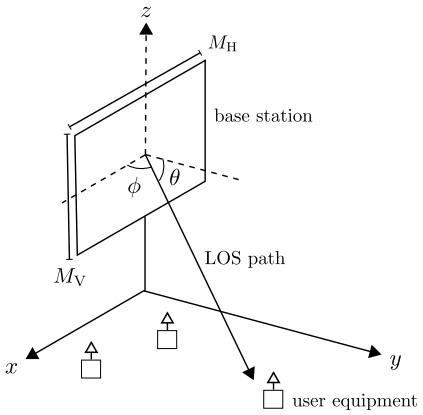

Fig. 1. Illustration of the BS and its geometry. Angles ϕ and θ denote azimuth and elevation, respectively.

notation, and $\otimes$ denotes the tensor product (also known as Kronecker product). The notation $[\boldsymbol{v}]_{\mathcal{I}}$ represents the vector obtained by selecting the elements of $\boldsymbol{v}$ that corresponds to the index set $\mathcal{I}$.

II. System Model

We consider a single-cell massive MIMO system with a BS serving U single-antenna user equipment (UEs). The system operates on perfectly-synchronized time division duplexing (TDD) and the uplink-downlink channel reciprocity assumption holds. The BS is equipped with a URA of size $M_{\mathrm{BS}} = M_{\mathrm{H}} \cdot M_{\mathrm{V}}$, as illustrated in Figure 1. Considering the downlink operation, the BS employs precoding filters $\boldsymbol{f}_u[n] \in \mathbb{C}^{M_{\mathrm{BS}} \times 1}$ to serve a data stream $s_u[n]$ to each UE u at each transmission time interval (TTI) n. Let $\boldsymbol{h}_u[n] \in \mathbb{C}^{M_{\mathrm{BS}} \times 1}$ denote the downlink channel vector. Then, the received signal by the UE u at TTI n can be expressed as

$$y_u[n] = \boldsymbol{h}_u^{\mathsf{H}}[n]\boldsymbol{f}_u[n]s_u[n] + \sum_{j \neq u}^{U} \boldsymbol{h}_u^{\mathsf{H}}\boldsymbol{f}_j[n]s_j[n] + b_u[n], \quad (1)$$

where $b_u[n]$ denotes a zero mean complex-valued additive white Gaussian noise (AWGN) component. We assume that $\mathbb{E}[s_u[m]s_j^*[n]] = \delta(u-j)\cdot\delta(m-n)$ and $\mathbb{E}[b_u[m]b_j^*[n]] = \sigma_b^2 \cdot \delta(u-j)\cdot\delta(m-n)$. The average BS transmit power constraint can be expressed as $\sum_{u=1}^{U} E_{\mathrm{Tx},u} \leq E_{\mathrm{Tx}}$, with $E_{\mathrm{Tx},u} = \|\boldsymbol{f}_u[n]\|_2^2$ denoting the power allocated to UE u, and $E_{\mathrm{Tx}} \geq 0$ the total transmit power. The precoding filters are optimized based on imperfect CSI, as we will explain in more details in Section II-C. We define the downlink signal to noise ratio (SNR) as $\gamma_{\mathrm{DL}} = E_{\mathrm{Tx}}/\sigma_b^2$.

A. Channel Model

We assume Rician flat fading channel model such that

$$\boldsymbol{h}_u[n] = \sqrt{\frac{K}{K+1}}\boldsymbol{h}_u^{\mathrm{LOS}}[n] + \sqrt{\frac{1}{K+1}}\boldsymbol{h}_u^{\mathrm{NLOS}}[n] \in \mathbb{C}^{M_{\mathrm{BS}} \times 1}, \quad (2)$$

where $K \geq 0$ denotes the Rician K-factor, $\boldsymbol{h}_u^{\mathrm{LOS}}[n]$ the line of sight (LOS) component, and $\boldsymbol{h}_u^{\mathrm{NLOS}}[n]$ the non-line of sight (NLOS) component. Note that K controls the influence of the LOS term over the NLOS one.

The LOS component is determined by a Doppler phase shift $\psi_u[n]$ and an array steering vector $\boldsymbol{a}_u[n] \in \mathbb{C}^{M_{\mathrm{BS}} \times 1}$. Both components depend on the UE location and on its velocity relative to the BS. Let us first define some geometrical notation to describe the Doppler phase shift. Let $\boldsymbol{p}_{\mathrm{BS}}[n] \in \mathbb{R}^3$ and $\boldsymbol{p}_{\mathrm{UE},u}[n] \in \mathbb{R}^3$ denote the 3-dimensional position vectors of the BS and UE u, respectively. The BS-UE u distance vector is defined as $\boldsymbol{d}_u[n] = \boldsymbol{p}_{\mathrm{UE},u}[n] - \boldsymbol{p}_{\mathrm{BS}}[n]$, and is normalized as

$$\tilde{\boldsymbol{d}}_u[n] = \frac{\boldsymbol{d}_u[n]}{\|\boldsymbol{d}_u[n]\|_2} = \left[\tilde{d}_u^x[n], \tilde{d}_u^y[n], \tilde{d}_u^z[n]\right]^{\mathsf{T}}. \quad (3)$$

As illustrated in Figure 1, the respective elevation and azimuth angles of UE u at TTI n are given by

$$\overline{\theta}_u[n] = \arcsin \tilde{d}_u^z[n], \quad \overline{\phi}_u[n] = \arctan\left(\frac{\tilde{d}_u^y[n]}{\tilde{d}_u^x[n]}\right). \quad (4)$$

Assuming a certain random angle spread, the geometrical elevation and azimuth angles in (4) are modeled as

$$\theta_u[n] = \overline{\theta}_u[n] + X_\theta[n] \quad (5)$$

$$\phi_u[n] = \overline{\phi}_u[n] + X_\phi[n], \quad (6)$$

where $X_\theta[n]$ and $X_\phi[n]$ denote real-valued independent and identically distributed Gaussian random variables with zero mean and variance σ_θ^2 and σ_ϕ^2, respectively. Define the LOS wave vector as [17]

$$\boldsymbol{k}_u[n] = \frac{2\pi}{\lambda}[\cos\theta_u[n]\cos\phi_u[n], \cos\theta_u[n]\sin\phi_u[n], \sin\theta_u[n]]^{\mathsf{T}}, \quad (7)$$

where λ denotes the carrier wavelength. Furthermore, let $\boldsymbol{v}_u[n] \in \mathbb{R}^3$ denote the speed vector of UE u relative to the fixed BS. The Doppler phase shift is finally defined as $\psi_u[n] = \boldsymbol{k}_u^{\mathsf{T}}[n]\boldsymbol{v}_u[n]$. The steering vector definition depends on how the antenna array elements are arranged in space. Considering a URA placed in the x-z plane as illustrated in Figure 1, the m-th element of the steering vector is given by [17]

$$[\boldsymbol{a}_u[n]]_m = \sqrt{g_{u,m}[n]} \cdot e^{-\jmath(\delta_{m_{\mathrm{H}}}^{(u)}[n] + \xi_{m_{\mathrm{V}}}^{(u)}[n])} \quad (8)$$

$$\delta_{m_{\mathrm{H}}}^{(u)}[n] = \frac{2\pi}{\lambda} d_{\mathrm{H}}(m_{\mathrm{H}} - 1)\cos\theta_u[n]\cos\phi_u[n] \quad (9)$$

$$\xi_{m_{\mathrm{V}}}^{(u)}[n] = \frac{2\pi}{\lambda} d_{\mathrm{V}}(m_{\mathrm{V}} - 1)\sin\theta_u[n] \quad (10)$$

$$m = m_{\mathrm{V}} + (m_{\mathrm{H}} - 1)\cdot M_{\mathrm{V}} \quad (11)$$

$$m_{\mathrm{V}} \in \{1, \ldots, M_{\mathrm{V}}\}, \quad m_{\mathrm{H}} \in \{1, \ldots, M_{\mathrm{H}}\}, \quad (12)$$

with $g_{u,m}[n]$ representing the m-th antenna element gain, and d_{H} and d_{V} the horizontal and vertical inter-antenna spacing, respectively. Note that the antenna gain $g_{u,m}[n]$ is a function of $\theta_u[n]$ and $\phi_u[n]$. From (8), it follows that

$$\boldsymbol{a}_u[n] = \boldsymbol{G}_u[n](\boldsymbol{a}_{\mathrm{H},u}[n] \otimes \boldsymbol{a}_{\mathrm{V},u}[n]), \quad (13)$$

where $\boldsymbol{G}_u[n] = \mathrm{Diag}(\sqrt{g_{u,1}[n]}, \ldots, \sqrt{g_{u,M_{\mathrm{BS}}}[n]})$ stands for the M_{BS}-dimensional diagonal antenna gains matrix. The vectors $\boldsymbol{a}_{\mathrm{H},u}[n] \in \mathbb{C}^{M_{\mathrm{H}} \times 1}$ and $\boldsymbol{a}_{\mathrm{V},u}[n] \in \mathbb{C}^{M_{\mathrm{V}} \times 1}$ represent the horizontal and vertical sub-array steering vectors, respectively. Their elements are defined as

$$[\boldsymbol{a}_{\mathrm{H},u}[n]]_{m_{\mathrm{H}}} = e^{-\jmath\delta_{m_{\mathrm{H}}}^{(u)}[n]}, \quad [\boldsymbol{a}_{\mathrm{V},u}[n]]_{m_{\mathrm{V}}} = e^{-\jmath\xi_{m_{\mathrm{V}}}^{(u)}[n]}. \quad (14)$$

for $m_{\mathrm{H}} \in \{1,\dots,M_{\mathrm{H}}\}$, and $m_{\mathrm{V}} \in \{1,\dots,M_{\mathrm{V}}\}$. Finally, the LOS component can be expressed as

$$\boldsymbol{h}_u^{\mathrm{LOS}}[n] = e^{\jmath\psi_u[n]} \cdot \boldsymbol{a}_u[n] \tag{15a}$$

$$= e^{\jmath\psi_u[n]} \cdot \boldsymbol{G}_u[n](\boldsymbol{a}_{\mathrm{H},u}[n] \otimes \boldsymbol{a}_{\mathrm{V},u}[n]). \tag{15b}$$

The NLOS component consists of diffuse background scattering components modeled as Rayleigh fading. To model the fading time evolution, the fading is modeled as a first-order Gauss-Markov process [18]. Hence, the NLOS component is given by

$$\boldsymbol{h}_u^{\mathrm{NLOS}}[n+1] = \rho_u[n]\boldsymbol{h}_u^{\mathrm{NLOS}}[n] + \sqrt{1-\rho_u^2[n]}\boldsymbol{h}_{\mathcal{N}}, \tag{16}$$

where $\boldsymbol{h}_{\mathcal{N}}$ is a zero mean circularly symmetric Gaussian (ZMCSG) random vector with spatial covariance matrix $\boldsymbol{R}_{\mathcal{N}}$, and $\rho_u[n]$ denotes the temporal correlation parameter. Considering the Clarke-Jakes autocorrelation model, it follows that $\rho_u[n] = J_0(2\pi f_{\mathrm{D},u}[n]T_s)$, with $J_0(\cdot)$ representing the zeroth-order Bessel function, $f_{\mathrm{D},u}[n] = \|\boldsymbol{v}_u[n]\|_2/\lambda$, the maximum Doppler shift, and T_s the TTI length.

B. Sub-Array Representation

The algebraic structure of (13) allows us to obtain the individual contributions of $\boldsymbol{a}_{\mathrm{H},u}[n]$ and $\boldsymbol{a}_{\mathrm{V},u}[n]$ by carefully selecting the elements of $\boldsymbol{h}_u[n]$. We define the respective horizontal and vertical sub-array index sets as

$$\mathcal{I}_{\mathrm{H}} = \{1 + (m_{\mathrm{H}}-1)M_{\mathrm{V}} \,|\, m_h = 1,\dots,M_{\mathrm{H}}\} \tag{17}$$

$$\mathcal{I}_{\mathrm{V}} = \{1,\dots,M_{\mathrm{V}}\}. \tag{18}$$

Also, we define the M_{H}-dimensional horizontal sub-array channel vector as

$$\boldsymbol{h}_{\mathrm{H},u}[n] = [\boldsymbol{h}_u[n]]_{\mathcal{I}_{\mathrm{H}}} = \sqrt{\frac{K}{K+1}}\boldsymbol{h}_{\mathrm{H},u}^{\mathrm{LOS}}[n] + \sqrt{\frac{1}{K+1}}\boldsymbol{h}_{\mathrm{H},u}^{\mathrm{NLOS}}[n] \tag{19}$$

$$\boldsymbol{h}_{\mathrm{H},u}^{\mathrm{LOS}}[n] = e^{\jmath\psi_u[n]} \cdot \boldsymbol{G}_{\mathrm{H}}[n]\boldsymbol{a}_{\mathrm{H},u}[n], \quad \boldsymbol{h}_{\mathrm{H},u}^{\mathrm{NLOS}}[n] = \left[\boldsymbol{h}_u^{\mathrm{NLOS}}[n]\right]_{\mathcal{I}_{\mathrm{H}}}$$

$$\boldsymbol{G}_{\mathrm{H}}[n] = \mathrm{Diag}(\sqrt{g_{u,m}[n]}), \forall m \in \mathcal{I}_{\mathrm{H}}$$

and the M_{V}-dimensional vertical sub-array channel vector as

$$\boldsymbol{h}_{\mathrm{V},u}[n] = [\boldsymbol{h}_u[n]]_{\mathcal{I}_{\mathrm{V}}} = \sqrt{\frac{K}{K+1}}\boldsymbol{h}_{\mathrm{V},u}^{\mathrm{LOS}}[n] + \sqrt{\frac{1}{K+1}}\boldsymbol{h}_{\mathrm{V},u}^{\mathrm{NLOS}}[n] \tag{20}$$

$$\boldsymbol{h}_{\mathrm{V},u}^{\mathrm{LOS}}[n] = e^{\jmath\psi_u[n]} \cdot \boldsymbol{G}_{\mathrm{V}}[n]\boldsymbol{a}_{\mathrm{V},u}[n], \quad \boldsymbol{h}_{\mathrm{V},u}^{\mathrm{NLOS}}[n] = \left[\boldsymbol{h}_u^{\mathrm{NLOS}}[n]\right]_{\mathcal{I}_{\mathrm{V}}}$$

$$\boldsymbol{G}_{\mathrm{V}}[n] = \mathrm{Diag}(\sqrt{g_{u,m}[n]}), \forall m \in \mathcal{I}_{\mathrm{V}}$$

Note that the sub-array channel vectors are obtained from $\boldsymbol{h}_u[n]$ by simply selecting the corresponding vector elements.

C. CSI Acquisition

In TDD systems with calibrated radio-frequency (RF) front-ends, the downlink channels are reciprocal to the uplink channels. Therefore, the BS may obtain channel estimates from pilot sequences transmitted in uplink training slots. Let $\boldsymbol{p}_u = [p_u[0],\dots,p_u[L-1]]^{\mathsf{T}}$ denote the length-L pilot sequence of UE u. We assume that the pilot sequences follow an orthogonal design, i.e., $\boldsymbol{p}_i^{\mathsf{H}}\boldsymbol{p}_j = L \cdot \delta(i-j)$. This orthogonality property can be found in many sequences, for example, discrete Fourier transform (DFT) and Zadoff-Chu sequences. During the uplink training TTI n, the UEs simultaneously transmit their pilot sequences to the BS with power E_{P}. Thus, the received signal at the BS can be written as

$$\boldsymbol{X}[n] = \sqrt{E_{\mathrm{P}}}\sum_{u=1}^{U}\boldsymbol{h}_u[n]\boldsymbol{p}_u^{\mathsf{H}}[n] + \boldsymbol{B}[n] \in \mathbb{C}^{M_{\mathrm{BS}}\times L}, \tag{21}$$

with $\boldsymbol{B}[n] \in \mathbb{C}^{M_{\mathrm{BS}}\times L}$ denoting the uplink complex-valued AWGN term. The elements of the noise matrix are modeled as ZMCSG random variables with variance σ_b^2. From (21), the least squares (LS) estimate of the UE u channel vector is given by

$$\hat{\boldsymbol{h}}_u[n] = \frac{1}{L\sqrt{E_{\mathrm{P}}}}\boldsymbol{X}[n]\boldsymbol{p}_u[n] = \boldsymbol{h}_u[n] + \frac{1}{L\sqrt{E_{\mathrm{P}}}}\boldsymbol{B}[n]\boldsymbol{p}_u[n]. \tag{22}$$

We define the uplink SNR as $\gamma_{\mathrm{UL}} = E_{\mathrm{P}}/\sigma_b^2$.

III. Precoding Methods

This section begins with a brief review of the classical MRT and ZF precoders. Then, these classical precoding schemes are reformulated considering the tensor approach in Section III-B. Unlike previous works [14] that rely on the explicit channel separability, the proposed TMRT and TZF precoders are based on the tensor factorization of the intended and interfering UEs' subspaces. Our results on the factorization of these subspaces are the main theoretical contribution of this paper and they are discussed in Theorems 1 and 2. Finally, the CSI requirements and the computational complexity of the proposed precoders are discussed in Section III-D.

A. Linear Precoders

1) Maximum Ratio Transmition (MRT): The MRT precoder $\boldsymbol{f}_{\mathrm{MRT},u}[n]$ is designed to maximize the received signal power at the intended user [19]. From the Cauchy-Schwarz inequality, the MRT precoder is given by

$$\boldsymbol{f}_{\mathrm{MRT},u}[n] = \underset{\boldsymbol{f},\|\boldsymbol{f}\|_2^2=E_{\mathrm{Tx},u}}{\arg\max}\left|\boldsymbol{h}_u[n]^{\mathsf{H}}\boldsymbol{f}\right|^2 = \frac{\sqrt{E_{\mathrm{Tx},u}}}{\|\boldsymbol{h}_u[n]\|_2}\boldsymbol{h}_u[n], \tag{23}$$

Note that the MRT precoder does not attempt to cancel the multi-user interference.

2) Zero-Forcing (ZF): The ZF precoder $\boldsymbol{f}_{\mathrm{ZF},u}[n]$ is designed to satisfy the zero multi-user interference condition:

$$\tilde{\boldsymbol{H}}_u[n]\boldsymbol{f}_{\mathrm{ZF},u}[n] = \boldsymbol{0}_{(U-1)\times 1}, \tag{24}$$

where

$$\tilde{\boldsymbol{H}}_u[n] = [\boldsymbol{h}_1[n],\dots,\boldsymbol{h}_{u-1}[n],\boldsymbol{h}_{u+1}[n],\dots,\boldsymbol{h}_U[n]]^{\mathsf{H}} \tag{25}$$

denotes the $(U-1)\times M_{\mathrm{BS}}$-dimensional multi-user interference channel matrix relative to UE u. This condition can be satisfied by projecting the MRT precoder onto the null-space of the matrix $\tilde{\boldsymbol{H}}_u[n]$ if $M_{\mathrm{BS}} \geq U$ [20]. To this end, consider the following eigenvalue decomposition:

$$\tilde{\boldsymbol{H}}_u^{\mathsf{H}}[n]\tilde{\boldsymbol{H}}_u[n] = \boldsymbol{V}_u[n]\boldsymbol{\Lambda}_u[n]\boldsymbol{V}_u^{\mathsf{H}}[n], \tag{26}$$

with $\boldsymbol{V}_u[n] \in \mathbb{C}^{M_{\mathrm{BS}}\times M_{\mathrm{BS}}}$ denoting the eigenvector matrix, and $\boldsymbol{\Lambda}_u[n] \in \mathbb{C}^{M_{\mathrm{BS}}\times M_{\mathrm{BS}}}$ the diagonal eigenvalue matrix. The null-space projector can be expressed as

$$\boldsymbol{P}_u[n] = \boldsymbol{I}_{M_{\mathrm{BS}}} - \tilde{\boldsymbol{V}}_u[n]\tilde{\boldsymbol{V}}_u^{\mathsf{H}}[n] \in \mathbb{C}^{M_{\mathrm{BS}}\times M_{\mathrm{BS}}}, \tag{27}$$

where $\tilde{\boldsymbol{V}}_u[n] \in \mathbb{C}^{M_{\text{BS}} \times (U-1)}$ is formed by the $U-1$ dominant eigenvectors of (26). The ZF precoder is then given by:

$$\tilde{\boldsymbol{f}}_u[n] = \boldsymbol{P}_u[n]\boldsymbol{h}_u[n] \tag{28}$$

$$\boldsymbol{f}_{\text{ZF},u}[n] = \frac{\sqrt{E_{\text{Tx},u}}}{\|\tilde{\boldsymbol{f}}_u[n]\|_2}\tilde{\boldsymbol{f}}_u[n]. \tag{29}$$

B. Tensor Precoders

1) Tensor Maximum Ratio Transmission (TMRT): The TMRT precoder is built upon the separability of the subspace spanned by $\boldsymbol{h}_u[n]$ presented in Theorem 1. To support the demonstration of this result, we present the following two lemmas.

Lemma 1. *For sufficiently large Rician-K factors, $\boldsymbol{h}_u[n]$, $\boldsymbol{h}_{H,u}[n]$, and $\boldsymbol{h}_{V,u}[n]$ may be well-approximated as*

$$\boldsymbol{h}_u[n] \approx \boldsymbol{h}_u^{LOS}[n] = e^{j\psi_u[n]} \cdot \boldsymbol{G}_u[n](\boldsymbol{a}_{H,u}[n] \otimes \boldsymbol{a}_{V,u}[n]) \tag{30}$$

$$\boldsymbol{h}_{H,u}[n] \approx \boldsymbol{h}_{H,u}^{LOS}[n] = e^{j\psi_u[n]} \cdot \boldsymbol{G}_{H,u}[n]\boldsymbol{a}_{H,u}[n] \tag{31}$$

$$\boldsymbol{h}_{V,u}[n] \approx \boldsymbol{h}_{V,u}^{LOS}[n] = e^{j\psi_u[n]} \cdot \boldsymbol{G}_{V,u}[n]\boldsymbol{a}_{V,u}[n] \tag{32}$$

Proof. The NLOS terms become insignificant relative to the LOS terms for sufficiently large Rician-K factors. Therefore, the considered approximation holds. □

Lemma 2. *The respective basis vectors of the subspaces spanned by the approximations in* (30)–(32) *are given by $\boldsymbol{a}_{H,u}[n] \otimes \boldsymbol{a}_{V,u}[n]$, $\boldsymbol{a}_{H,u}[n]$, and $\boldsymbol{a}_{V,u}[n]$ if the diagonal antenna gain matrices $\boldsymbol{G}_u[n]$, $\boldsymbol{G}_{H,u}[n]$, and $\boldsymbol{G}_{V,u}[n]$ are non-singular.*

Proof. This result follows from the fact that the Doppler shift and the antenna gain matrices do not change the direction of the corresponding steering vectors. □

Theorem 1. *For sufficiently large Rician-K factors, the subspace spanned by $\boldsymbol{h}_u[n]$ consists of the tensor product between the subspaces generated by $\boldsymbol{h}_{H,u}[n]$ and $\boldsymbol{h}_{V,u}[n]$.*

Proof. Lemmas 1 and 2 demonstrate that the basis vector of the subspace spanned by $\boldsymbol{h}_u[n]$ is given by the tensor product between $\boldsymbol{a}_{\text{H},u}[n]$ and $\boldsymbol{a}_{\text{V},u}[n]$. Furthermore, these steering vectors form bases for the subspaces generated by $\boldsymbol{h}_{\text{H},u}[n]$ and $\boldsymbol{h}_{\text{V},u}[n]$, respectively. □

Remark. *The channel vector $\boldsymbol{h}_u[n]$ cannot be factorized into a tensor product between $\boldsymbol{h}_{H,u}[n]$ and $\boldsymbol{h}_{V,u}[n]$ in general because*

1) *The Rayleigh NLOS term $\boldsymbol{h}_u^{NLOS}[n]$ does not have any specific separable structure;*
2) *The antenna gains matrix $\boldsymbol{G}_u[n]$ cannot be decomposed into elevation and azimuth factors.*

However, Theorem 1 shows that the 1*-dimensional subspace spanned by $\boldsymbol{h}_u[n]$ can be factorized if the conditions provided in Lemmas 1 and 2 are satisfied, as illustrated in Figure 2.*

Based on Theorem 1, the TMRT precoder consists of designing sub-array precoders $\tilde{\boldsymbol{f}}_{\text{H},u}[n]$ and $\tilde{\boldsymbol{f}}_{\text{V},u}[n]$ that maximize the received power at the intended UE and then combining them through the tensor product as

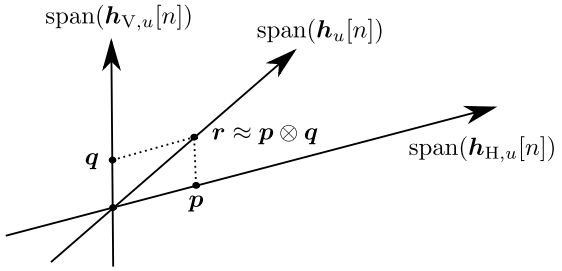

Fig. 2. Illustration of Theorem 1. The vector $\boldsymbol{r} \in \text{span}(\boldsymbol{h}_u[n])$ can be well approximated by the tensor product between $\boldsymbol{p} \in \text{span}(\boldsymbol{h}_{\text{H},u}[n])$ and $\boldsymbol{q} \in \text{span}(\boldsymbol{h}_{\text{V},u}[n])$.

$$\boldsymbol{f}_{\text{TMRT},u}[n] = \tilde{\boldsymbol{f}}_{\text{H},u}[n] \otimes \tilde{\boldsymbol{f}}_{\text{V},u}[n] \tag{33}$$

$$\tilde{\boldsymbol{f}}_{\text{H},u}[n] = \underset{\boldsymbol{f}_{\text{H}}, \|\boldsymbol{f}_{\text{H}}\|_2^2 = E_{\text{Tx},u}^{1/2}}{\arg\max} |\boldsymbol{h}_{\text{H},u}[n]\boldsymbol{f}_{\text{H}}|^2 = \frac{\sqrt[4]{E_{\text{Tx},u}}}{\|\boldsymbol{h}_{\text{H},u}[n]\|_2}\boldsymbol{h}_{\text{H},u}[n] \tag{34}$$

$$\tilde{\boldsymbol{f}}_{\text{V},u}[n] = \underset{\boldsymbol{f}_{\text{V}}, \|\boldsymbol{f}_{\text{V}}\|_2^2 = E_{\text{Tx},u}^{1/2}}{\arg\max} |\boldsymbol{h}_{\text{H},u}[n]\boldsymbol{f}_{\text{V}}|^2 = \frac{\sqrt[4]{E_{\text{Tx},u}}}{\|\boldsymbol{h}_{\text{V},u}[n]\|_2}\boldsymbol{h}_{\text{V},u}[n]. \tag{35}$$

2) Tensor Zero-Forcing (TZF): The TZF precoder is formulated based on the results of Theorem 2 and of Corollary 1. To support these results, we present Lemmas 3–5. For future convenience, let us define the horizontal and vertical multi-user interference channel matrices

$$\tilde{\boldsymbol{H}}_{\text{H},u}[n] = [\boldsymbol{h}_{\text{H},1}[n], \ldots, \boldsymbol{h}_{\text{H},u-1}[n], \boldsymbol{h}_{\text{H},u+1}[n], \ldots, \boldsymbol{h}_{\text{H},U}[n]]^{\mathsf{H}} \tag{39}$$

$$\tilde{\boldsymbol{H}}_{\text{V},u}[n] = [\boldsymbol{h}_{\text{V},1}[n], \ldots, \boldsymbol{h}_{\text{V},u-1}[n], \boldsymbol{h}_{\text{V},u+1}[n], \ldots, \boldsymbol{h}_{\text{V},U}[n]]^{\mathsf{H}} \tag{40}$$

with dimensions $(U-1) \times M_{\text{H}}$ and $(U-1) \times M_{\text{V}}$, respectively, and the Gram matrices in (36)–(38), shown on the top of the next page.

Lemma 3. *For sufficiently large Rician-K factors, the Gram matrices* (36)–(38) *can be well approximated as*

$$\tilde{\boldsymbol{H}}_u^{\mathsf{H}}[n]\tilde{\boldsymbol{H}}_u[n] \approx \sum_{j \neq u}^{U} \boldsymbol{G}_j[n]\boldsymbol{R}_j[n]\boldsymbol{G}_j[n] \tag{41}$$

$$\tilde{\boldsymbol{H}}_{H,u}^{\mathsf{H}}[n]\tilde{\boldsymbol{H}}_{H,u}[n] \approx \sum_{j \neq u}^{U} \boldsymbol{G}_{H,j}[n]\boldsymbol{R}_{H,j}[n]\boldsymbol{G}_{H,j}[n] \tag{42}$$

$$\tilde{\boldsymbol{H}}_{V,u}^{\mathsf{H}}[n]\tilde{\boldsymbol{H}}_{V,u}[n] \approx \sum_{j \neq u}^{U} \boldsymbol{G}_{V,j}[n]\boldsymbol{R}_{V,j}[n]\boldsymbol{G}_{V,j}[n], \tag{43}$$

with

$$\boldsymbol{R}_j[n] = \boldsymbol{R}_{H,j}[n] \otimes \boldsymbol{R}_{V,j}[n] \in \mathbb{C}^{M_{BS} \times M_{BS}} \tag{44}$$

$$\boldsymbol{R}_{H,j}[n] = \boldsymbol{a}_{H,j}[n]\boldsymbol{a}_{H,j}[n]^{\mathsf{H}} \in \mathbb{C}^{M_H \times M_H} \tag{45}$$

$$\boldsymbol{R}_{V,j}[n] = \boldsymbol{a}_{V,j}[n]\boldsymbol{a}_{V,j}[n]^{\mathsf{H}} \in \mathbb{C}^{M_V \times M_V} \tag{46}$$

Proof. The approximations in (41)–(43) are obtained by noticing that the NLOS and NLOS-LOS cross terms in (36)–(38) are negligible compared to the LOS component for sufficiently

$$\tilde{\boldsymbol{H}}_u^{\mathsf{H}}[n]\tilde{\boldsymbol{H}}_u[n] = \sum_{j\neq u}^{U}\left(\frac{K}{K+1}\boldsymbol{h}_j^{\text{LOS}}[n]\boldsymbol{h}_j^{\text{LOS}}[n]^{\mathsf{H}} + \frac{\sqrt{K}}{K+1}\boldsymbol{h}_j^{\text{LOS}}[n]\boldsymbol{h}_j^{\text{NLOS}}[n]^{\mathsf{H}} + \frac{\sqrt{K}}{K+1}\boldsymbol{h}_j^{\text{NLOS}}[n]\boldsymbol{h}_j^{\text{LOS}}[n]^{\mathsf{H}} + \frac{1}{K+1}\boldsymbol{h}_j^{\text{NLOS}}[n]\boldsymbol{h}_j^{\text{NLOS}}[n]^{\mathsf{H}}\right) \quad (36)$$

$$\tilde{\boldsymbol{H}}_{\text{H},u}^{\mathsf{H}}[n]\tilde{\boldsymbol{H}}_{\text{H},u}[n] = \sum_{j\neq u}^{U}\left(\frac{K}{K+1}\boldsymbol{h}_{\text{H},j}^{\text{LOS}}[n]\boldsymbol{h}_{\text{H},j}^{\text{LOS}}[n]^{\mathsf{H}} + \frac{\sqrt{K}}{K+1}\boldsymbol{h}_{\text{H},j}^{\text{LOS}}[n]\boldsymbol{h}_{\text{H},j}^{\text{NLOS}}[n]^{\mathsf{H}} + \frac{\sqrt{K}}{K+1}\boldsymbol{h}_{\text{H},j}^{\text{NLOS}}[n]\boldsymbol{h}_{\text{H},j}^{\text{LOS}}[n]^{\mathsf{H}} + \frac{1}{K+1}\boldsymbol{h}_{\text{H},j}^{\text{NLOS}}[n]\boldsymbol{h}_{\text{H},j}^{\text{NLOS}}[n]^{\mathsf{H}}\right) \quad (37)$$

$$\tilde{\boldsymbol{H}}_{\text{V},u}^{\mathsf{H}}[n]\tilde{\boldsymbol{H}}_{\text{V},u}[n] = \sum_{j\neq u}^{U}\left(\frac{K}{K+1}\boldsymbol{h}_{\text{V},j}^{\text{LOS}}[n]\boldsymbol{h}_{\text{V},j}^{\text{LOS}}[n]^{\mathsf{H}} + \frac{\sqrt{K}}{K+1}\boldsymbol{h}_{\text{V},j}^{\text{LOS}}[n]\boldsymbol{h}_{\text{V},j}^{\text{NLOS}}[n]^{\mathsf{H}} + \frac{\sqrt{K}}{K+1}\boldsymbol{h}_{\text{V},j}^{\text{NLOS}}[n]\boldsymbol{h}_{\text{V},j}^{\text{LOS}}[n]^{\mathsf{H}} + \frac{1}{K+1}\boldsymbol{h}_{\text{V},j}^{\text{NLOS}}[n]\boldsymbol{h}_{\text{V},j}^{\text{NLOS}}[n]^{\mathsf{H}}\right) \quad (38)$$

large Rician-K factors. In (41), $\boldsymbol{R}_j[n]$ is obtained by applying the mixed-product property of the tensor product [21] as:

$$\begin{aligned}\boldsymbol{R}_j[n] &= \left(\boldsymbol{a}_{\text{H},j}[n]\otimes\boldsymbol{a}_{\text{V},j}[n]\right)\left(\boldsymbol{a}_{\text{H},j}[n]\otimes\boldsymbol{a}_{\text{V},j}[n]\right)^{\mathsf{H}} &(47a)\\ &= \left(\boldsymbol{a}_{\text{H},j}[n]\boldsymbol{a}_{\text{H},j}[n]^{\mathsf{H}}\right)\otimes\left(\boldsymbol{a}_{\text{V},j}[n]\boldsymbol{a}_{\text{V},j}[n]^{\mathsf{H}}\right) &(47b)\\ &= \boldsymbol{R}_{\text{H},j}[n]\otimes\boldsymbol{R}_{\text{V},j}[n] &(47c)\end{aligned}$$

□

Lemma 4. *The approximations* (41)–(43) *and the matrices*

$$\boldsymbol{\Theta}_u[n] = \sum_{j\neq u}^{U}\boldsymbol{R}_j[n] \quad (48)$$

$$\boldsymbol{\Theta}_{H,u}[n] = \sum_{j\neq u}^{U}\boldsymbol{R}_{H,j}[n] \quad (49)$$

$$\boldsymbol{\Theta}_{V,u}[n] = \sum_{j\neq u}^{U}\boldsymbol{R}_{V,j}[n] \quad (50)$$

span the same column-spaces, respectively, if the diagonal antenna gains matrices $\boldsymbol{G}_j[n]$, $\boldsymbol{G}_{H,j}[n]$, and $\boldsymbol{G}_{V,j}[n]$ are non-singular.

Proof. The non-singular scaling performed by the diagonal antenna gains matrices in (41)–(43) do not change the direction of the eigenvectors of $\boldsymbol{R}_j[n]$, $\boldsymbol{R}_{\text{H},j}[n]$, and $\boldsymbol{R}_{\text{V},j}[n]$. □

Lemma 5. *The column-space of $\boldsymbol{\Theta}_u[n]$ can be factorized into the tensor product between the column-spaces of $\boldsymbol{\Theta}_{H,u}[n]$ and $\boldsymbol{\Theta}_{V,u}[n]$ if the elevation angles that locate the interfering UEs are approximately equal.*

Proof. By inserting (44) into (48), we have

$$\boldsymbol{\Theta}_u[n] = \sum_{j\neq u}^{U}\boldsymbol{R}_{\text{H},j}[n]\otimes\boldsymbol{R}_{\text{V},j}[n]. \quad (51)$$

If the interfering users' elevation angles $\theta_j[n]$ are alike, then the matrices $\boldsymbol{R}_{\text{V},j}[n]$ are almost equivalent for all $j\neq u$. This assumption allows us to approximately factorize (51) as

$$\boldsymbol{\Theta}_u[n] \approx \left(\sum_{j\neq u}^{U}\boldsymbol{R}_{\text{H},j}[n]\right)\otimes\boldsymbol{\Theta}_{\text{V},u}[n] = \boldsymbol{\Theta}_{\text{H},u}[n]\otimes\boldsymbol{\Theta}_{\text{V},u}[n]. \quad (52)$$

□

Theorem 2. *If the elevation angles that locate the interfering UEs are sufficiently close and if the Rician-K factor is sufficiently large, then the column-space of $\tilde{\boldsymbol{H}}_u^{\mathsf{H}}[n]\tilde{\boldsymbol{H}}_u[n]$ is approximately formed by the tensor product of the column-spaces of $\tilde{\boldsymbol{H}}_{H,u}^{\mathsf{H}}[n]\tilde{\boldsymbol{H}}_{H,u}[n]$ and $\tilde{\boldsymbol{H}}_{V,u}^{\mathsf{H}}[n]\tilde{\boldsymbol{H}}_{V,u}[n]$.*

Proof. Lemmas 3 and 4 demonstrate that the column-spaces of (41)–(43) and (48)–(50) are approximately the same for sufficiently large Rician-K factors, respectively. Lemma 5 shows that the subspaces of (41)–(43) are connected through a tensor product. Therefore, the column-space of $\tilde{\boldsymbol{H}}_u^{\mathsf{H}}[n]\tilde{\boldsymbol{H}}_u[n]$ is spanned by the tensor product between $\tilde{\boldsymbol{H}}_{\text{H},u}^{\mathsf{H}}[n]\tilde{\boldsymbol{H}}_{\text{H},u}[n]$ and $\tilde{\boldsymbol{H}}_{\text{V},u}^{\mathsf{H}}[n]\tilde{\boldsymbol{H}}_{\text{V},u}[n]$. □

Corollary 1. *Let the matrices $\boldsymbol{K}$, $\boldsymbol{K}_H$, and $\boldsymbol{K}_V$ denote projectors to the column-spaces of $\tilde{\boldsymbol{H}}_u^{\mathsf{H}}[n]\tilde{\boldsymbol{H}}_u[n]$, $\tilde{\boldsymbol{H}}_{H,u}^{\mathsf{H}}[n]\tilde{\boldsymbol{H}}_{H,u}[n]$, and $\tilde{\boldsymbol{H}}_{V,u}^{\mathsf{H}}[n]\tilde{\boldsymbol{H}}_{V,u}[n]$, respectively. If the conditions of Theorem 2 hold, then $\boldsymbol{K}\approx\boldsymbol{K}_H\otimes\boldsymbol{K}_V$.*

As in the classical ZF precoder, we build a projector to the null-space of the multi-user interference channel matrix $\tilde{\boldsymbol{H}}_u[n]$ using the results of Theorem 2 and Corollary 1. First, consider the eigenvalue decompositions of (37) and (38)

$$\tilde{\boldsymbol{H}}_{\text{H},u}^{\mathsf{H}}[n]\tilde{\boldsymbol{H}}_{\text{H},u}[n] = \boldsymbol{V}_{\text{H},u}[n]\boldsymbol{\Lambda}_{\text{H},u}[n]\boldsymbol{V}_{\text{H},u}^{\mathsf{H}}[n] \quad (53)$$

$$\tilde{\boldsymbol{H}}_{\text{V},u}^{\mathsf{H}}[n]\tilde{\boldsymbol{H}}_{\text{V},u}[n] = \boldsymbol{V}_{\text{V},u}[n]\boldsymbol{\Lambda}_{\text{V},u}[n]\boldsymbol{V}_{\text{V},u}^{\mathsf{H}}[n], \quad (54)$$

and the corresponding column-space projectors

$$\boldsymbol{K}_{\text{H},u}[n] = \tilde{\boldsymbol{V}}_{\text{H},u}[n]\tilde{\boldsymbol{V}}_{\text{H},u}^{\mathsf{H}}[n]\in\mathbb{C}^{M_{\text{H}}\times M_{\text{H}}} \quad (55)$$

$$\boldsymbol{K}_{\text{V},u}[n] = \tilde{\boldsymbol{V}}_{\text{V},u}[n]\tilde{\boldsymbol{V}}_{\text{V},u}^{\mathsf{H}}[n]\in\mathbb{C}^{M_{\text{V}}\times M_{\text{V}}}, \quad (56)$$

where $\tilde{\boldsymbol{V}}_{\text{H},u}[n]\in\mathbb{C}^{M_{\text{H}}\times(U-1)}$ and $\tilde{\boldsymbol{V}}_{\text{V},u}[n]\in\mathbb{C}^{M_{\text{V}}\times(U-1)}$ contain the $U-1$ dominant eigenvectors of $\boldsymbol{V}_{\text{H},u}[n]$ and $\boldsymbol{V}_{\text{V},u}[n]$, respectively. From Corollary 1, the column-space projector of $\tilde{\boldsymbol{H}}_u^{\mathsf{H}}[n]\tilde{\boldsymbol{H}}_u[n]$ may be approximated as $\boldsymbol{K}\approx\boldsymbol{K}_{\text{H}}\otimes\boldsymbol{K}_{\text{V}}$. Then, the null-space projector (27) can be approximated as

$$\boldsymbol{P}_u[n]\approx\boldsymbol{P}_{\text{TZF},u}[n] = \boldsymbol{I}_{M_{\text{BS}}} - \boldsymbol{K}_{\text{H},u}[n]\otimes\boldsymbol{K}_{\text{V},u}[n]. \quad (57)$$

Motivated by Theorem 1, we project the tensor product $\boldsymbol{h}_{\text{H},u}[n]\otimes\boldsymbol{h}_{\text{V,u}}[n]$ onto the multi-user interference channel matrix's null space. Hence, the TZF precoder is then given by

$$\overline{\boldsymbol{f}}_u[n] = \boldsymbol{P}_{\text{TZF},u}[n](\boldsymbol{h}_{\text{H},u}[n]\otimes\boldsymbol{h}_{\text{V,u}}[n]) \quad (58)$$

$$\boldsymbol{f}_{\text{TZF},u}[n] = \frac{\sqrt{E_{\text{Tx},u}}}{\|\overline{\boldsymbol{f}}_u[n]\|_2}\overline{\boldsymbol{f}}_u[n]. \quad (59)$$

Note that the null spaces of (53) and (54) exist if and only if M_{H} and M_{V} are larger than $U-1$. Therefore, the feasibility condition for the TZF precoder can be formulated as $\min(M_{\text{H}},M_{\text{V}})>U-1$.

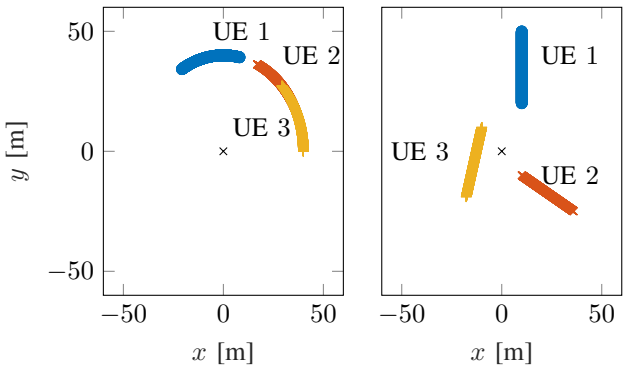

Fig. 3. Circular (left) and linear (right) tracks. The BS array is located at $(0, 0, 25)$ m and the height of each UE is 1.5 m.

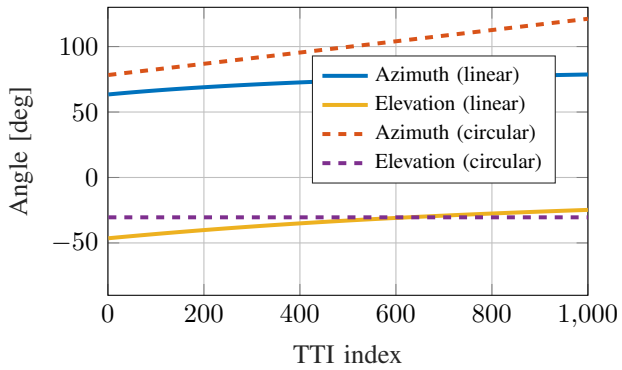

Fig. 4. Angles for linear and circular tracks of UE 1.

C. CSI Requirements

The CSI typically required by linear precoders is the intended UE channel vector $\boldsymbol{h}_u[n]$ and possibly the interfering ones $\{\boldsymbol{h}_j[n] \,|\, j = 1, \ldots, U, j \neq u\}$. This information can be obtained as detailed in Section II-C, for example. By contrast the proposed tensor precoders are based only on the M_{H}- and M_{V}-dimensional sub-array channel vectors $\boldsymbol{h}_{\mathrm{H},u}[n]$ and $\boldsymbol{h}_{\mathrm{V},u}[n]$, respectively. The total number of parameters to be estimated by the tensor approach is proportional to $M_{\mathrm{H}} + M_{\mathrm{V}}$, while that number is proportional to $M_{\mathrm{H}} \cdot M_{\mathrm{V}}$ in the linear approach. Therefore, the tensor approach is less expensive than the linear one, as the CSI acquisition cost is usually proportional to the number of channel coefficients.

D. Complexity Analysis

The MRT precoder performs $2M_{\mathrm{BS}} + 1$ operations, and the TMRT precoder carries out additional M_{BS} multiplications due to the tensor product, $3M_{\mathrm{BS}} + 1$ in total. Therefore, the linear and tensor MRT precoders are comparable in terms of number of computations. The computational complexity of the ZF-based precoders is dominated by the calculation of the projection matrices. The number of multiplications required by this calculation is cubic with the channel vector length. Therefore, the ZF precoder performs $O(M_{\mathrm{BS}}^3) = O((M_{\mathrm{H}} \cdot M_{\mathrm{V}})^3)$ multiplications, whereas the TZF only $O(M_{\mathrm{H}}^3) + O(M_{\mathrm{V}}^3)$.

IV. Simulations

In this section, we present simulation results to evaluate the channel subspace separability results and the proposed tensor precoders. We assume a single BS with a half-wavelength URA of $M_{\mathrm{BS}} = 16 \times 16$ isotropic antennas serving $U = 3$ single-antenna UEs. The TDD frames are divided into uplink and downlink slots with TTI of 1 ms, and the carrier frequency is 6 GHz. The uplink and downlink SNR are 20 dB and 10 dB, respectively, and the LOS angle spreads in (5), (6) are $\sigma_\theta = \sigma_\phi = 1^\circ$. We consider the circular and linear tracks depicted in Figure 3 for the UE trajectories. The modulus of the UE speed vectors is constant $\|\boldsymbol{v}_u\|_2 = 30$ m/s for $u = 1, 2, 3$. The elevation and azimuth angles corresponding to the trajectory of UE 1 during 1000 TTIs (= 1 second) are shown in Figure 4. In the circular track, we observe that the elevation angle remains constant, whereas the azimuth angle grows. This track is therefore useful for investigating the evolution of the horizontal and vertical subspaces. The linear track describes a more realistic scenario, where both azimuth and elevation angles grow.

In the first experiment scenario, we investigate the evolution of subspaces spanned by the channel vectors $\boldsymbol{h}_u[n]$, $\boldsymbol{h}_{\mathrm{H},u}[n]$, and $\boldsymbol{h}_{\mathrm{V},u}[n]$. To quantify the subspace evolution, we consider the chordal distance between the dominant eigenvectors of the channel correlation matrices. More specifically, the chordal distance between the eigenvectors $\boldsymbol{u}[m]$ and $\boldsymbol{u}[n]$ of same length is defined as $d_{\mathrm{C}}^2(\boldsymbol{u}[m], \boldsymbol{u}[n]) = 1 - \left|\boldsymbol{u}^{\mathsf{H}}[m]\boldsymbol{u}[n]\right|^2$ [22]. In Figure 5, the chordal distance is calculated relative to the eigenvector at TTI $n = 0$ for the subspaces of the full, horizontal, and vertical channel vectors. The eigenvectors are estimated by averaging 256 channel realizations for each TTI. The chordal distances relative to $\boldsymbol{h}_1[n]$, $\boldsymbol{h}_{\mathrm{H},1}[n]$, and $\boldsymbol{h}_{\mathrm{V},1}[n]$ are plotted in Figure 5 for Rician-K factors of 0 dB and 20 dB considering the circular track. This result suggests that the vertical component, which corresponds to the elevation angle, remains constant, while the full and horizontal components evolve in time. This behavior is observed for both Rician-K factors. We extend this experiment to evaluate the column-space evolution of the multi-user interference channel matrices (36)–(38). These matrices are calculated relative to UE 1 assuming the circular track scenario and $K = 20$ dB for all UEs, as depicted in Figure 3. This result indicates that the column-space of the multi-user interfering channel matrix does not evolve. This is because the interfering UEs are characterized by the same elevation angle. Therefore, the approximation in Lemma 3 holds and the conditions given in Theorem 2 are satisfied.

In the second experiment scenario, we evaluate the proposed tensor precoders for both circular and linear tracks and $K = 20$ dB. As observed in Figures 5 and 6 for the circular track, the elevation component evolves slowly relative to the azimuth component. In this case, it is reasonable to think that it is not necessary to update the vertical precoders as often as the horizontal precoders. To test this hypothesis, we carried out experiments where the precoders are designed at uplink slots (allocated every 250 TTIs) and employed in the successive downlink slots. At each uplink TTI, the BS acquires the CSI of each UE as described in Section II-C, designs the benchmark linear precoder (MRT or ZF) and the corresponding tensor

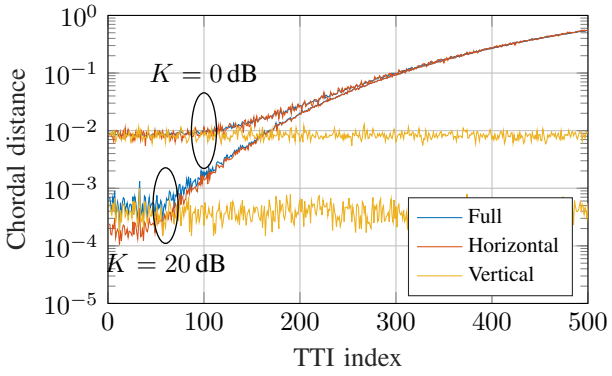

Fig. 5. Chordal distance evolution of channel subspace with circular tracks.

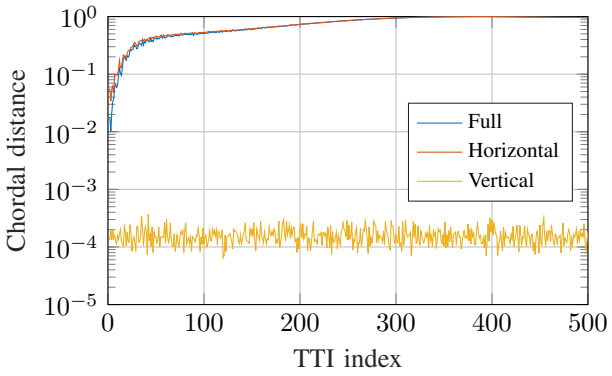

Fig. 6. Chordal distance of multi-user interference channel subspace with circular tracks, $K = 20$ dB.

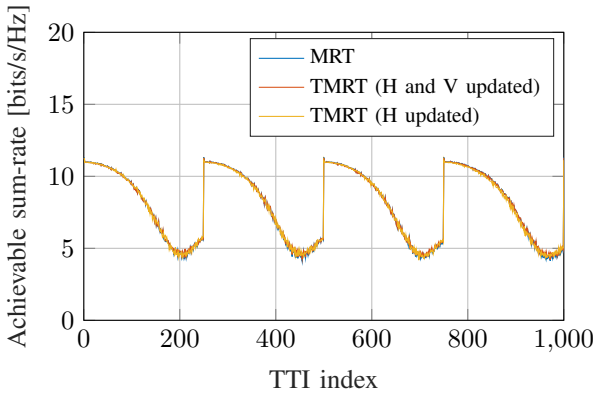

Fig. 7. MRT-based precoders performance with circular tracks.

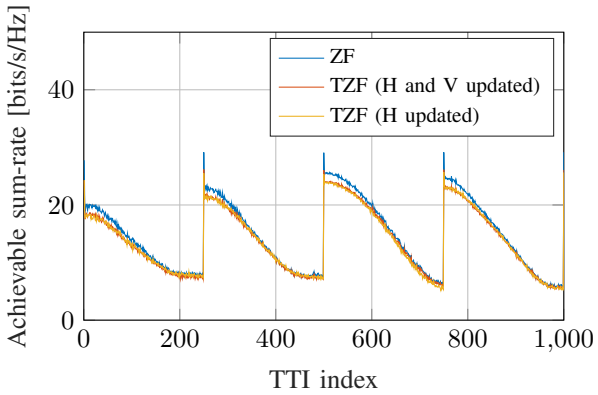

Fig. 8. ZF-based precoders performance with circular tracks.

precoder. We consider two implementations of the tensor precoders. The standard implementation consists of updating both horizontal (H) and vertical (V) tensor precoder filters at each uplink slot. The second implementation, by contrast, calculates the vertical component at the first uplink slot and, afterward, updates only the horizontal component.

In Figures 7 and 8, the MRT- and ZF-based precoders are evaluated for circular tracks, respectively. As observed in Figures 5 and 6, the elevation subspace does not change in circular tracks. Consequently, implementations of the TMRT and TZF precoders perform the same. Figure 7 shows that the linear and tensor approaches exhibit the same performance, empirically confirming the validity of Theorem 1. Regarding the ZF-based precoders in Figure 8, we observe that the tensor precoders exhibit a small loss compared to the linear precoders.

Figures 9 and 10 show the performance of the MRT- and ZF-based precoders for linear tracks, respectively. In this scenario, both elevation and azimuth components evolve in time, and therefore, the corresponding precoders need to be updated at each uplink slot. These figures indicate that the tensor precoders face an important performance loss when only the horizontal precoders are updated. However, the loss relative to their linear counterparts is insignificant when both horizontal and vertical components are updated. These results demonstrate that the proposed tensor precoders may be applied to any kind of UE track to approximate their linear counterpart when both horizontal and vertical components are updated.

In the previous experiments, we have analyzed the precoders in terms of the achievable sum-rate. The ZF-based precoders are evaluated in terms of the empirical cumulative distribution function (cdf) of the precoder runtime in Figure 11. This figure reveals that the tensor approach is roughly twice as fast as its linear counterpart. Therefore, TZF strikes an excellent rate-complexity trade-off.

V. Conclusion

In this paper, we present novel results concerning the subspace separability of Rician channels, and, based on these results, we propose efficient tensor precoders. We assess the validity of the subspace separability and the performance of the proposed precoders through computer simulations. The TMRT and TZF precoders can closely approximate their linear counterparts while exhibiting a much lower computational complexity. Specifically, the TZF precoder is twice as fast as the ZF precoder, while exhibiting a negligible rate loss in a very dynamic communication scenario.

We considered a single specular LOS component, which is adequate for specific scenarios, i.e., millimeter wave systems with a strong LOS component. We plan to extend the proposed tensor precoding framework to manage communication scenarios with multiple specular components and multi-antenna receivers.

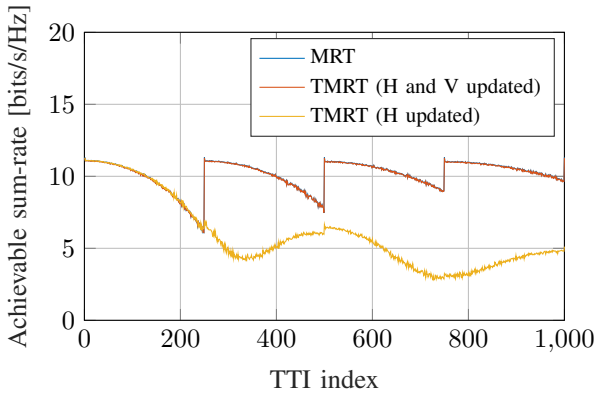

Fig. 9. MRT-based precoders performance with linear tracks.

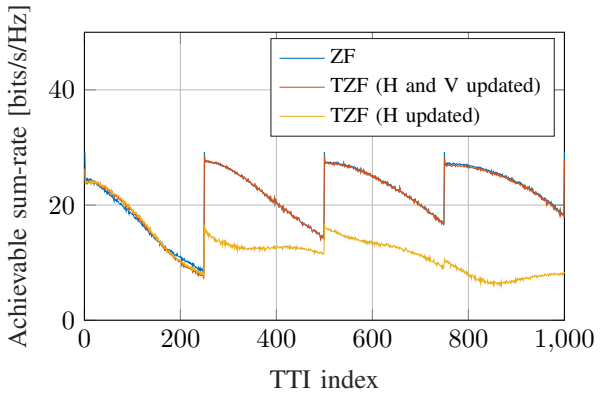

Fig. 10. ZF-based precoders performance with linear tracks.

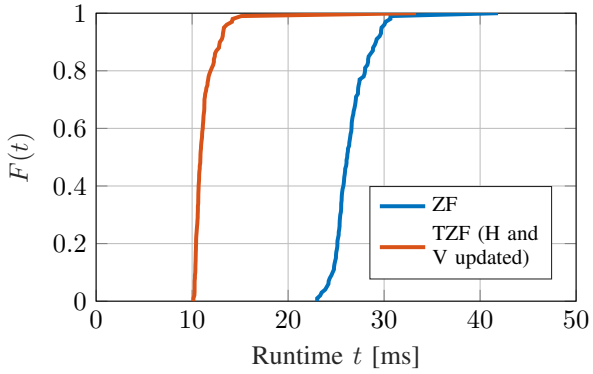

Fig. 11. Empirical cdf of runtime.

REFERENCES

[1] T. L. Marzetta, *Fundamentals of massive MIMO*. Cambridge University Press, 2016.

[2] L. Van der Perre, L. Liu, and E. G. Larsson, "Efficient DSP and Circuit Architectures for Massive MIMO: State of the Art and Future Directions," *IEEE Transactions on Signal Processing*, vol. 66, no. 18, pp. 4717–4736, Sep. 2018.

[3] D. Ying, F. W. Vook, T. A. Thomas, D. J. Love, and A. Ghosh, "Kronecker product correlation model and limited feedback codebook design in a 3D channel model," in *Proc. IEEE ICC'14*, Sydney, NSW, Jun. 2014, pp. 5865–5870.

[4] S. Qiu, Da Chen, D. Qu, K. Luo, and T. Jiang, "Downlink Precoding With Mixed Statistical and Imperfect Instantaneous CSI for Massive MIMO Systems," *IEEE Transactions on Vehicular Technology*, vol. 67, no. 4, pp. 3028–3041, Apr. 2018.

[5] S. Schwarz, "Robust full-dimension MIMO transmission based on limited feedback angular-domain CSIT," *EURASIP Journal on Wireless Communications and Networking*, vol. 2018, no. 1, p. 58, Dec. 2018.

[6] C. Zhang, Y. Jing, Y. Huang, and L. Yang, "Performance Analysis for Massive MIMO Downlink With Low Complexity Approximate Zero-Forcing Precoding," *IEEE Transactions on Communications*, vol. 66, no. 9, pp. 3848–3864, Sep. 2018.

[7] S. Kashyap, C. Mollen, E. Bjornson, and E. G. Larsson, "Frequency-domain interpolation of the zero-forcing matrix in massive MIMO-OFDM," in *Proc. IEEE SPAWC'16*, Edinburgh, United Kingdom, Jul. 2016, pp. 1–5.

[8] K. Li, R. R. Sharan, Y. Chen, T. Goldstein, J. R. Cavallaro, and C. Studer, "Decentralized Baseband Processing for Massive MU-MIMO Systems," *IEEE Journal on Emerging and Selected Topics in Circuits and Systems*, vol. 7, no. 4, pp. 491–507, Dec. 2017.

[9] A. Alkhateeb, G. Leus, and R. W. Heath, "Multi-Layer Precoding: A Potential Solution for Full-Dimensional Massive MIMO Systems," *IEEE Transactions on Wireless Communications*, vol. 16, no. 9, pp. 5810–5824, Sep. 2017.

[10] L. N. Ribeiro, S. Schwarz, and A. L. F. de Almeida, "Double-Sided Massive MIMO Transceivers for mmWave Communications," *IEEE Access*, vol. 7, pp. 157 667–157 679, 2019.

[11] L. N. Ribeiro, A. L. F. de Almeida, and J. C. M. Mota, "Identification of separable systems using trilinear filtering," in *Proc. IEEE CAMSAP'15*, Cancún, Mexico, Dec. 2015, pp. 189–192.

[12] L. N. Ribeiro, S. Schwarz, M. Rupp, A. L. F. de Almeida, and J. C. M. Mota, "A low-complexity equalizer for massive MIMO systems based on array separability," in *Proc. EUSIPCO'17*, Kos, Greece, Aug. 2017, pp. 2453–2457.

[13] L. N. Ribeiro, A. L. F. de Almeida, and J. C. M. Mota, "Separable linearly constrained minimum variance beamformers," *Signal Processing*, vol. 158, pp. 15–25, May 2019.

[14] ——, "Low-Rank Tensor MMSE Equalization," in *Proc. ISWCS'19*, Oulu, Finland, Aug. 2019, pp. 511–516.

[15] Z. Wang, W. Liu, C. Qian, S. Chen, and L. Hanzo, "Two-Dimensional Precoding for 3-D Massive MIMO," *IEEE Transactions on Vehicular Technology*, vol. 66, no. 6, pp. 5485–5490, Jun. 2017.

[16] G. Zhu, K. Huang, V. K. N. Lau, B. Xia, X. Li, and S. Zhang, "Hybrid Beamforming via the Kronecker Decomposition for the Millimeter-Wave Massive MIMO Systems," *IEEE Journal on Selected Areas in Communications*, vol. 35, no. 9, pp. 2097–2114, Sep. 2017.

[17] H. L. Van Trees, *Optimum array processing: Part IV of detection, estimation and modulation theory*. Wiley Online Library, 2002, vol. 1.

[18] K. T. Truong and R. W. Heath, "Effects of channel aging in massive MIMO systems," *Journal of Communications and Networks*, vol. 15, no. 4, pp. 338–351, Aug. 2013.

[19] E. Bjornson, M. Bengtsson, and B. Ottersten, "Optimal Multiuser Transmit Beamforming: A Difficult Problem with a Simple Solution Structure [Lecture Notes]," *IEEE Signal Processing Magazine*, vol. 31, no. 4, pp. 142–148, Jul. 2014.

[20] Q. H. Spencer, A. L. Swindlehurst, and M. Haardt, "Zero-forcing methods for downlink spatial multiplexing in multiuser MIMO channels," *IEEE Transactions on Signal Processing*, vol. 52, no. 2, pp. 461–471, 2004.

[21] N. D. Sidiropoulos, L. De Lathauwer, X. Fu, K. Huang, E. E. Papalexakis, and C. Faloutsos, "Tensor Decomposition for Signal Processing and Machine Learning," *IEEE Transactions on Signal Processing*, vol. 65, no. 13, pp. 3551–3582, Jul. 2017.

[22] S. Schwarz and M. Rupp, "Performance evaluation of low complexity double-sided massive MIMO transceivers," in *Proc. IEEE CCNC'16*, Las Vegas, NV, USA, Jan. 2016, pp. 582–588.